Validation of a 3D culture model for toxicity studies in malignant and non-cancerous cells

Validering av en 3D-odlingsmodell för toxicitetsstudier i maligna och icke-cancerösa celler

Kajsa Andréasson Dahlgren

Lunds tekniska högskola (Faculty of Engineering), LTH
Master of Science in Engineering, Engineering Nanoscience
Department of Immunotechnology

Red Glead Discovery AB

2021

Abstract

Cancer is a widespread and commonly fatal disease in constant need of new treatments. Traditionally, new pharmaceuticals have been tested in 2D models. This is not ideal, as 2D environments do not reflect the *in vivo* milieu of the cells. Instead, it has been increasingly suggested to implement 3D models, which are thought to be more predictive of *in vivo* responses to treatment. It has been shown that cancerous cells are less sensitive to anti-cancer drugs when cultured in 3D. Thus, this study aimed to compare the effect of 2D and 3D environments on the potency of the MEK inhibitor trametinib in human cancerous A549 and non-cancerous LL47 cells. The 3D model used was an electrospun poly-caprolactone membrane, on which the cells were seeded and then treated with varying trametinib concentrations. The 2D model was a traditional cell culture plate. The study also investigated the mechanism of trametinib. It was shown that trametinib affects the amount of p-ERK, in line with data published by others. No statistically significant difference in potency could be shown between the models. However, after optimisation the 3D model itself was shown to be working and giving reproducible results, suggesting further use in preclinical studies.

Introduction

Cancer is one of the leading causes of death worldwide, resulting in nearly 10 million fatal cases as recently as in 2018 (1). There are several types of cancer, and it can affect all parts of the body. However, there have been suggestions for hallmarks common to all cancers (2). These hallmarks include continuous proliferative signalling, evasion of growth suppressors, resistance to cell death, induction of angiogenesis, activation of invasion and metastasis, and the ability to enable replicative immortality, as reviewed in (2). Another way to put this is by defining cancer cells by two heritable properties: cancer cells proliferate regardless of normal constraints and are able to invade, and remain in, locations meant for other cells (3). Other possible hallmarks that have been suggested are avoidance of immune destruction and abnormal, deregulated cellular metabolism (2, 3).

Cancer develops due to an accumulation of mutations, which is the reason for the uncontrolled proliferation – the normal checks and balances of the cells have been put out of play (3). This genetic instability has been dubbed an enabling characteristic of cancer, together with its ability to induce tumour-promoting inflammation (2). There are two main types of genes that are highly important for cancer: proto-oncogenes, in which mutations lead to hyperactivity (gain-of-function), and tumour suppressor genes, in which mutations lead to silencing of the gene (loss-of function) (3). For a proto-oncogene, whose resulting mutant version is called an oncogene, a mutation in only one gene copy is enough, while for tumour suppressor genes typically both copies need to be mutated to bring about the silencing effect (3).

To further complicate the idea of cancer developing as a result of accumulating mutations is the notion of oncogene addiction (4). This poses that it is not simply the sum of all mutations that bring forth the malignant phenotype, but rather that certain oncogenes are more important and that some cancers are highly dependent on these genes to maintain their malignancy. Such genes vary from cancer to cancer and may be involved in different functions of the cells. Connected to this oncogene addiction, cancer cells can also show signs of tumour suppression gene hypersensitivity, in which re-introduction of such a gene has a greater effect than expected if all mutations in the cancer were of equal importance (4). This kind of dependency on specific genes introduces an opportunity for treatment to target cancer cells with greater accuracy (5).

Other than the cancer cells themselves, the microenvironment of tumours includes several other cell types, and it is affected by intricate signalling pathways. The complexity of this system might even rival that of healthy tissues (2), and it is here the hallmarks and characteristics of angiogenesis induction, evasion of the immune system, and tumour-promoting inflammation come into play.

While there are many current treatments for different cancers, the mutability of the cells can quickly lead to resistance. Furthermore, as cancer cells mutate so readily, it is no guarantee that all cells within a patient – or even within a single tumour – will respond in the same way to the treatment given (3, 6). Therefore, there is a constant need for new and improved therapies.

As for the development of any new drug, anti-cancer agents are tested at an early stage in *in vitro* models, which typically include two-dimensional (2D) cell cultures (7). However, such models can be unreliable in their predictions of *in vivo* effects, and only about 5 % of the agents

that show desired activity in preclinical trials are licensed after phase III clinical testing (8). This is a much lower percentage than for other diseases (8), and it is costly both in time and economic terms for the pharmaceutical industry, as well as from a therapeutic and patient viewpoint, where new efficacious drugs are always in demand. One reason for this high failure rate is that the complexity of cancer *in vivo* is not reflected in most preclinical models – several physiological characteristics such as general tissue architecture, mechanical properties, and cell-to-cell and cell-to-matrix interactions, are lost (9).

A step that thus seems beneficial to take when it comes to improving the preclinical studies of cancer treatments is to switch from the traditional 2D cell cultures to a three-dimensional (3D) model that more closely resembles the *in vivo* environment of the cancer cells. Such models are thought to be more reliable when it comes to predicting *in vivo* toxicity and efficacy of drugs (7), and have been used to predict clinical response to drug treatment with high accuracy (10).

As stated above, there is a discrepancy between many preclinical models and cancer *in vivo* when it comes to several characteristics. This is a problem, for instance since it has been indicated that the attachment of cancer cells to the extracellular matrix (ECM) provides protection against drug-induced apoptosis (11). In 2D models, where the cells grow as monolayers on flat surfaces, such interactions may not be correctly provided (12), and this can then lead to incorrect assessments of drug efficacy. In 3D, the idea is that an *in vivo*-like structure of the environment can confer a more correct balance of interactions between the cells. While there are exceptions (13, 14), several studies have shown that increased doses of cytotoxic compounds are needed in a 3D culture compared to a 2D culture to get the same inhibitory effect (12, 14-19). The protective role of a three-dimensional environment is also evident in radiation treatment (20). This indicates that a 2D culture might overestimate the cytotoxicity of a drug, which could be an important reason why new drug candidates that show promise in such models are still likely to fail in clinical trials.

Another advantage of 3D models is that they may provide information on the invasiveness of the cancer cells (12). As mentioned earlier, one hallmark of cancer is the ability of tumours to disseminate and invade other parts of the body. Such migration has been shown to take place in 3D models (21). Cells in 2D cultures may also migrate, but this migration differs from the 3D version (22). It is possible that the simplicity of 2D can be a hindrance for metastasis studies in such models.

One promising 3D model is the use of electrospun fibre membranes. Electrospinning, beyond being a cost-effective method of fabrication, confers several advantages such as the possibility of co-spinning with for instance collagen to create hybrid materials (12), using similar surface treatments and coatings as used in 2D and the overall morphological similarity to the ECM (23). The ECM has fibres with diameters ranging from tens to several hundred nanometres, and these fibres are randomly oriented to form nonwoven meshes (24). Fibre size and orientation are both properties that electrospun membranes mimic well. Electrospun membranes can be made from a large range of polymers, and properties such as thickness, fibre diameter and pore size can be precisely tuned (23). Electrospinning also has a high level or reproducibility, which can be an issue with many other 3D models (7, 25).

In this study, electrospun membranes made of polycaprolactone (PCL) will be used to assess the effects of a 3D environment on response to anti-cancer drugs. Such membranes have previously been used for culture of both cancerous and non-cancerous cells, with promising results regarding a future use in preclinical studies (26-28).

One example of an already existing cancer treatment is the compound trametinib. Trametinib is a reversible, highly selective, allosteric inhibitor of MEK 1 and 2 (29), and it thus inhibits the MAPK pathway of the cells. This pathway is ultimately involved in cell proliferation, and due to mutations in various components it is often constitutively active in cancer cells, which is why it is a popular target in cancer therapy (3, 30). In some cancers, parts of it may even serve as the subjects for oncogene addiction. An overexpressed and activated MAPK pathway is also indicated to be involved in inducing the so called epithelial-mesenchymal transition (EMT) (31). For epithelial-derived cancers, which account for 90 % of human tumours (32), the EMT is thought to be very important to the ability of the cells to leave their original site and invade other tissues (2). It is the invasiveness of cancer that determines its malignancy, and furthermore the EMT has been shown to confer resistance to treatment (33-35). It can therefore be said that the EMT, and thus any cause of it, contributes to the dangerous character of cancer. Here, trametinib will be used to investigate the effects on drug potency of the 3D culture model compared to a traditional 2D model.

Materials and Methods

Cell lines and culture media

The cell lines used were human lung adenocarcinoma A549 cells and human lung fibroblast LL47 cells. Both cell lines were purchased from Sigma-Aldrich (Damstadt, Germany). The A549 cells harbour a KRAS mutation ($KRAS^{G12S}$) which results in a constitutively active MAPK pathway (15), as discussed in the introduction.

The cells were cultured in different media. The A549 cells were cultured in Kaign's modified Ham's F-12 medium, complemented with 10 % FBS and 1 % penicillin-streptomycin. The LL47 cells were cultured in the same modified F-12 medium, complemented with 15 % FBS, 1 % penicillin-streptomycin, 45 mg/l ascorbic acid and 18 mg/l inositol. The modified F-12 medium and penicillin-streptomycin (10 000 U/ml) were purchased from Thermo Fisher Scientific (Gibco) (Waltham, MA, USA). The FBS was purchased from the American Type Culture Collection (ATCC) (Manassas, VA, USA).

Both cell lines were maintained in a cell culture incubator at 37 °C and 5 % CO_2. When passaged, they were detached with 0.025 % trypsin-0.01 % EDTA (Thermo Fisher Scientific (Gibco)).

Materials

Cell proliferation reagent WST-1 was purchased from Roche (Basel, Switzerland), and was always used according to the manufacturers protocol. Trametinib was purchased from AK Scientific (Union City, CA, USA). Mouse anti-p-ERK antibodies (catalogue number 9106S) were purchased from Cell Signaling Technology (Danvers, MA, USA). Mouse anti-β-actin antibodies (catalogue number A2228, clone AC-74) were purchased from Sigma Aldrich. Goat anti-mouse antibodies (reference number 31450) were purchased from Thermo Fisher Scientific.

2D model

Cell growth rate

To help determine treatment durations and how to seed cells for future analyses, the growth rates of the cell lines were investigated. Cells were seeded at different densities in 6-well plates and manually counted after 24, 48 and 72 hours. This counting was performed using a Bürker chamber. The number of cells seeded was 100 000, 200 000 and 400 000 cells/well, seeded in duplicate wells. By then plotting the number of cells vs hours in culture and fitting an exponential regression to the data points, the doubling time of the cells could be estimated.

Investigating seeding density

In order to determine what cell seeding density would be most appropriate to use in subsequent dose-dependency experiments, the cells were first seeded at different densities in a 96-well plate. Cell numbers were then evaluated after 24, 48 and 72 hours using the WST-1 assay, following the

manufacturer's instructions. The aim was to find a seeding density that gave a strong assay readout within the assay range. To do this, the plates were also evaluated several times during the incubation with WST-1, to see what reading time produced the best signal. Each cell line was seeded as duplicates of the respective density. The seeding densities were 500, 1 000, 2 500, 5 000, 10 000, 25 000 and 30 000 cells/well. This setup also allowed for another estimation of the cells' doubling time, by plotting absorbance values vs incubation time and fitting exponential regressions to these curves.

Western blot

To investigate the action of trametinib on a protein level, cell lysates from treated and non-treated cells were analysed through Western blot. The cells were seeded in 6-well plates and treated with different trametinib concentrations (0.1 to 30 µM) for 72 hours. Control wells were treated only with 0.5 % DMSO. The cells were then lysed (50 mM Tris, 150 mM NaCl, 1 mM EDTA, 1%Triton-X100, 1 mM DTT, protease and phosphatase inhibitors) after indicated treatment and the lysates were run on a NuPAGE™ Bis-Tris gel 4–12% gradient gel (Thermo Fisher Scientific (Invitrogen)). The proteins were then transferred to a polyvinylidene fluoride (PVDF) membrane which was blocked in 5% BSA in PBST. After this, the membrane was incubated with the primary antibody (mouse anti-p-ERK, diluted 1:500) overnight and then incubated with species-specific secondary antibodies (goat anti-mouse, diluted 1:25 000) for 1 hour at room temperature. The membrane was visualized with the ECL SuperSignal™ West Pico PLUS Chemiluminescent Substrate (Thermo Fisher Scientific). The images were captured with iBright Western Blot Imaging Systems (Thermo Fisher Scientific) and were quantified with ImageJ (Java-based image processing program developed at the National Institutes of Health and the Laboratory for Optical and Computational Instrumentation). After stripping the membrane, anti-β-actin antibodies (diluted 1:20 000) were used as the loading control for all samples.

The treatment regimen performed to investigate the amount of p-ERK after trametinib treatment (as a single therapy) in (36) was also performed for the A549 cells, with the exception of one timepoint where the treatment was shortened from 12 to 8 hours. The cells were seeded in 6-well plates and then treated with varying trametinib concentrations (other than the ones previously used) for 24 hours, or treated with one trametinib concentration for varying amounts of time. Lysing of the samples, running the gel, protein transfer and incubation with antibodies was done as described above.

Response to trametinib – 2D

To investigate the effect of trametinib on LL47 and A549 cells in 2D, the cells were seeded in 96-well plates and treated for 72 hours. Based on the experiment described above, 1 000 cells were seeded per well. The cells were treated within two hours after seeding. The trametinib was dissolved in DMSO, with a final DMSO concentration of 0.5 % in the wells. The same DMSO concentration was also used in the control wells. The trametinib concentrations (eight in total) were prepared as a serial dilution and ranged from 0.03 to 100 µM. The responses to the treatment

were evaluated using the WST-1 assay and the data were processed and used to plot dose-response curves in the Microsoft® Excel add-in XLfit® (IDBS, Guildford, United Kingdom). This was done by calculating the obtained absorbance values as percentages inhibition and then using these values to fit a curve according to the four-parameter log-logistic model

$$y(x) = A + \frac{B-A}{1+(\frac{10^C}{x})^D} \quad (1)$$

where y is the predicted inhibition, x is the treatment dose, A is the minimum amount of inhibition, B is the maximum amount of inhibition, C is the log EC_{50} and D is the slope of the curve. In XLfit®, this is known as model 203. From these curves, the EC_{50} value (the potency) could be estimated.

3D model

Electrospun membrane

As stated, the 3D culture was performed on electrospun polycaprolactone membranes. These had an average fibre diameter of 700 nm and random fibre orientation. The membranes came fitted in the wells of 96-well plates, which were purchased from Cellevate AB (Lund, Sweden). Before seeding any cells, the wells (the membrane) were pre-treated with 70 % ethanol, rinsed twice with PBS and then soaked with cell media and incubated for at least 30 minutes, according to the manufacturer's instructions. This media was then removed, and the cells were seeded in fresh medium.

Response to trametinib – 3D

To investigate the effect of trametinib on LL47 and A549 cells in 3D, the dose-dependency experiment performed in 2D was repeated in the 96-well plates fitted with membrane inserts described above. Given the larger surface area of the membranes compared to the flat bottom of the 2D wells, 3 000 cells were seeded per 3D well (compared to 1 000 cells/well in 2D). The cells were treated for 72 hours, with the same trametinib and DMSO concentrations as in 2D. The trametinib was added within 2 hours after seeding of the cells, just like in the 2D experiment. The responses to the treatment were again evaluated using the WST-1 assay. However, as the membranes would interfere with the absorbance readings and following the manufacturer's recommendation, the contents of the wells were pipetted from the 3D-plate to a 2D 96-well plate before reading.

Statistics

The trametinib treatment in 96-well plates was repeated three times each in the 2D and 3D models. Statistical significance was investigated using a two-tailed t-test and a significance level of 0.05.

Results

2D model

Cell growth rate

The growth rates of the cells were investigated by seeding varying densities of cells in 6-well plates and manually counting the numbers of cells after 24, 48 and 72 hours. The results can be found in table 1 below. As the growth rate depends on the number of cells seeded, one rate is reported per seeding density. The A549 cells grow faster than the LL47 cells for the lower seeding densities, while the LL47 grows faster for the highest seeding density (400 000 cells/well). At this seeding density, the LL47 cells even reach a plateau in their growth after 72 hours (the growth rate is therefore based only on the first two timepoints).

Table 1. Estimations of doubling times for the cell lines A549 and LL47, based on manual counting after 24, 48 and 72 hours. Different seeding densities were investigated, as indicated in the table.

Doubling time, hours		
Cells/well	A549	LL47
100 000	20.4	24.5
200 000	24.5	26.5
400 000	29.7	17.0

Determination of proper seeding densities

To determine a proper cell seeding density to use for the dose-response experiments, the cell lines were first seeded at different densities in 96-well plates and their proliferation rates were evaluated using the WST-1 assay. Based on this, it was determined that both cell lines were to be seeded at 1 000 cells/well. With this seeding density, the doubling times for the cell lines were determined to be 25.5 and 34.1 hours for A549 and LL47, respectively.

Trametinib induces p-ERK rebound in KRAS mutant A549 cells grown in 2D

Trametinib, as a MEK inhibitor, should affect the amount of p-ERK in the cells. This was investigated with Western blots, where mouse anti-p-ERK antibodies were used to detect p-ERK, and mouse anti-actin antibodies were used to check the loading of the gel.

For the first blot, the cells were treated for 72 hours with the varying trametinib concentrations also used in the dose-response experiments (the six middle concentrations). Neither cell line showed a dose-dependent response in regards to the amount of p-ERK after this trametinib treatment. Based on this, it was decided to repeat a previously performed experiment on the A549 cells (see below).

For the second blot, the treatment regimen from (36) was performed. Here, the cells were treated either with varying trametinib concentrations (ranging from 30 to 480 nM) for 24 hours, or with one trametinib concentration (60 nM) for varying durations (1-24 hours). The results are shown in figure 1. The first of these investigations showed a slight decrease in the amount of p-

ERK when the trametinib concentration increased. The other investigation showed that the amount of p-ERK is decreased for the shorter treatments, but then increases after 8 and 24 hours. In both cases (varying dose and varying time), the controls (0 nM and 0 hours) show very little p-ERK.

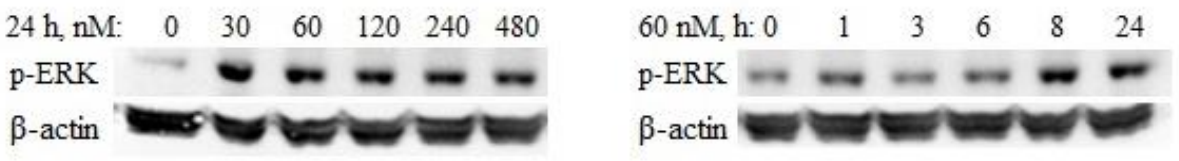

Figure 1. Western blot showing the amount of p-ERK in whole cell lysates after trametinib treatment with different concentrations (left) or for different durations (right). The lysates were from A549 cells grown in 2D, and the specific treatment (concentration and duration) is indicated in the figure. A slight decrease in p-ERK is seen when comparing the lowest and highest trametinib doses (left). When looking at the different treatment durations, there is an increase in p-ERK after 8 and 24 hours (right). For both cases, the controls (0 nM and 0 hours) show low amounts of p-ERK.

Similar trametinib potency in A549 and LL47 cells in 2D

To investigate the effect of trametinib on the cells in 2D, the cells were seeded in 96-well plates and treated with varying trametinib concentrations. The cell number was evaluated using the WST-1 assay after 72 hours.

After this 72 hour-treatment, both cell lines showed responses that were dose-dependent. However, it could be seen that the A549 data points adhered more closely to the theoretically fit regression, as compared to the LL47 (figures 2 and 3, respectively), indicating that this model of dose-dependency was more accurate for these cells. EC_{50} values were estimated for both cell lines (see also table 2 under 3D model below): 0.11 µM for the A549 cells and 0.16 µM for the LL47 cells. These values are not statistically significantly different from each other.

Interestingly, for almost all repeats and timepoints, the highest trametinib concentration (100 µM) gave much lower inhibition than the second highest concentration (30 µM), especially in the LL47 cells. This was disregarded as a form of outlier when the dose-response curves were plotted and the EC_{50} values estimated.

A549 (2D)

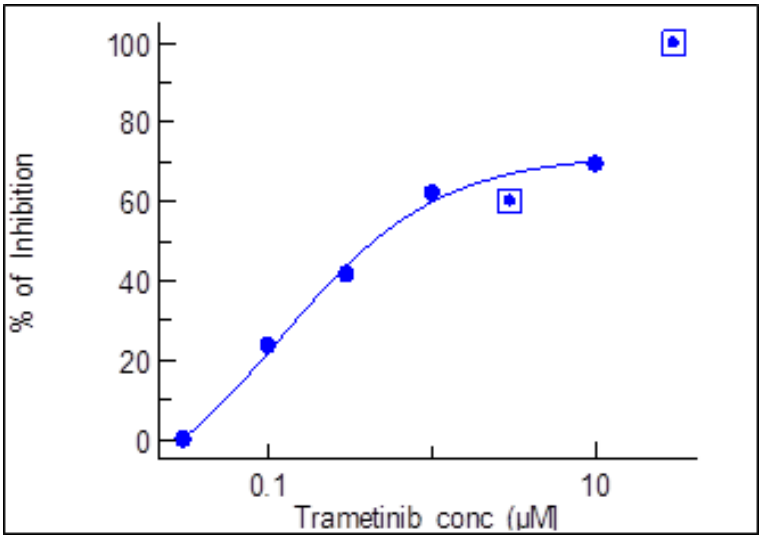

Figure 2. Dose-dependency curve showing the effect of trametinib as % inhibition vs concentration in A549 cells, in the traditional 2D model. The curve shown is a representative of the three repeats performed.

LL47 (2D)

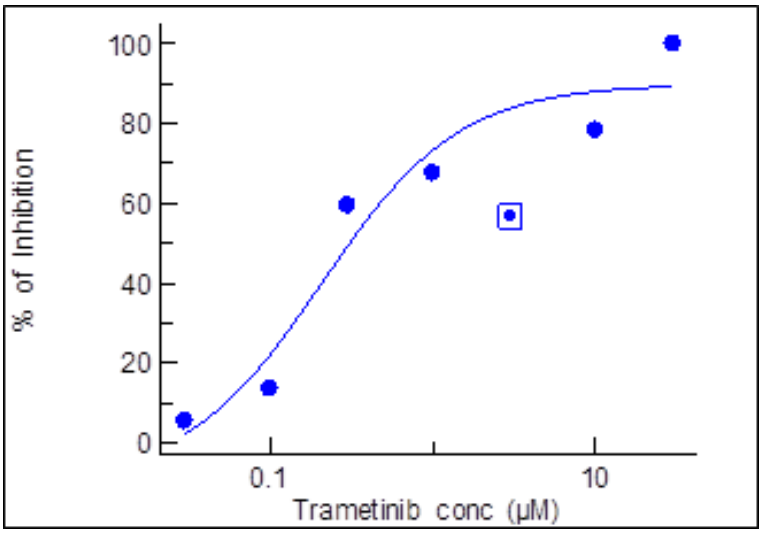

Figure 3. Dose-dependency curve showing the effect of trametinib as % inhibition vs concentration in LL47 cells, in the traditional 2D model. The curve shown is a representative of the three repeats performed.

3D model

Potency of trametinib remains unchanged when going from 2D to 3D

As in 2D, the cells were seeded in 96-well plates – here, the 3D plates with wells fitted with the PCL membrane – and treated with varying concentrations of trametinib to investigate the effects of the compound. After 72 hours of treatment, much like in 2D, both cell lines showed dose-dependent responses (figures 4 and 5). The EC_{50} values were estimated to be 0.11 µM in the A549 cells and 0.51 µM in the LL47 cells (see also table 2). These values are not statistically significantly different from each other, nor from the corresponding values obtained in 2D.

Something that did differ from the 2D results however is that the LL47 data points adhere more closely to the theoretical curve, i.e. the fit is better for these experiments. Another difference compared to the 2D is that the highest concentration (100 µM) tended to give the highest inhibition in 3D, while it in 2D often gave a much lower inhibition than the second highest concentration (30 µM). However, these values were not used in 3D either, as they were regarded as outliers here as well.

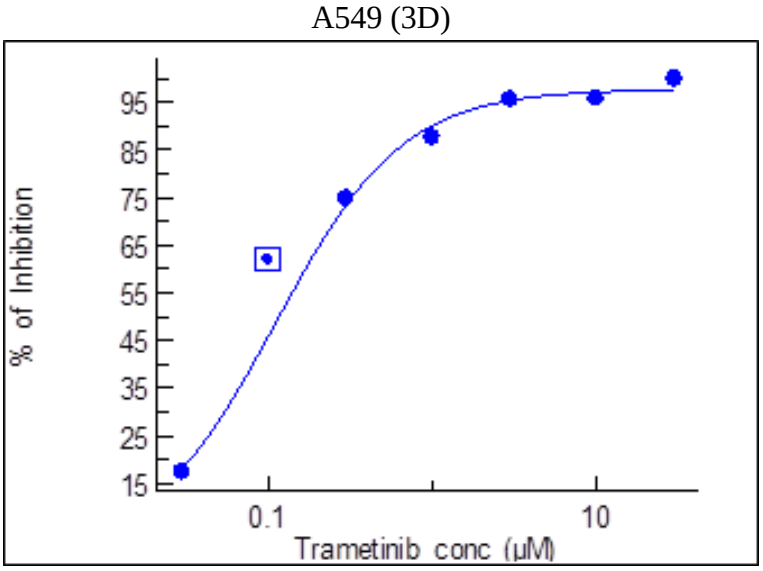

Figure 4. Dose-dependency curve showing the effect of trametinib as % inhibition vs concentration in A549 cells, in the 3D model. The curve shown is a representative of the three repeats performed.

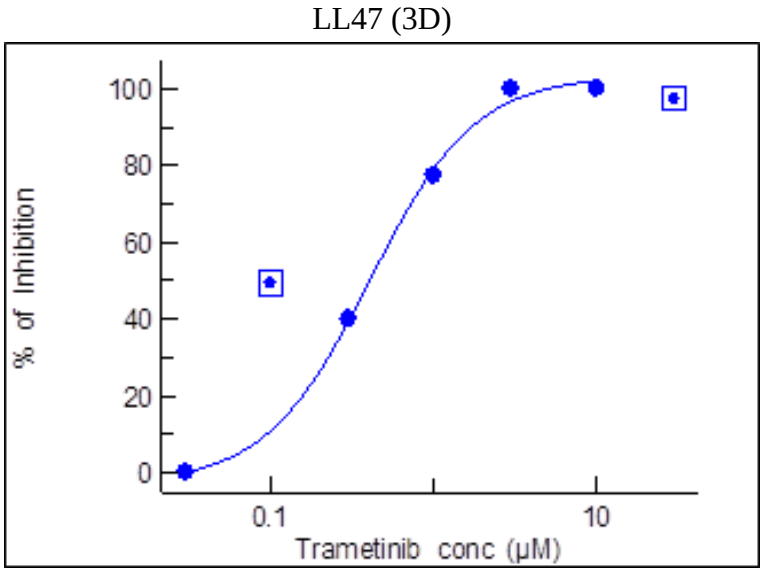

Figure 5. Dose-dependency curve showing the effect of trametinib as % inhibition vs concentration in LL47 cells, in the 3D model. The curve shown is a representative of the three repeats performed.

Table 2. EC_{50} values estimated by fitting the experimental data to a theoretical model (see Materials and methods). Values are in μM and are presented as mean ± standard deviation (based on three repeats). There is no statistically significant difference between the two cell lines, nor between the 2D and 3D model.

EC_{50} (μM)	2D	3D
A549	0.11 ± 0.016	0.11 ± 0.0015
LL47	0.16 ± 0.037	0.51 ± 0.39

Discussion

This study investigated the effects of a 2D vs 3D environment on the potency of the MEK inhibitor trametinib in cancerous A549 and non-cancerous LL47 cells. This was done by treating the cells with varying trametinib concentrations and evaluating cell viability via the colorimetric WST-1 assay. As trametinib is a MEK inhibitor, the amount of p-ERK in the cells was also investigated via Western blots. In general, the potency of trametinib was no different in 3D compared to in 2D. There was also no difference in the potency when comparing the two cell lines, which both displayed dose-dependent responses. However, in 2D the A549 cells, as compared to the LL47 cells, showed a more reproducible dose-dependency, which adhered more to the theoretical model that was fit to the data. In 3D, this difference between the cell lines was not observed. The Western blots showed that trametinib had an effect on the amount of p-ERK in the KRAS-mutated A549 cells, and that this effect decreased when treatment was prolonged.

At the beginning of the study, the growth rates of the two cell lines were investigated by manual counting. As summarised in table 1, the A549 cells grew faster than the LL47 cells, except for when 400 000 cells were seeded per well. This makes sense as the A549, being cancerous cells, are less dependent on normal cell-to-cell signalling for their proliferation and may therefore be able to grow fast regardless of such signalling. Once the LL47 cells became more crowded, they could proliferate faster, even reaching a plateau indicating contact inhibition. Contact inhibition is not present in various cancers (2), which could explain why the A549 cells never slowed down. However, these cells are also smaller than the LL47 and furthermore did not reach the same number of cells. The A549 cells may as well have reached such a plateau at a timepoint longer than 72 hours.

When the seeding density in 96-well plates was investigated on the other hand, it became clear that both cell lines were overcrowded at the two highest seeding densities. Here, there was a decrease in signal with time. As there was still more area per cell seeded in these smaller wells compared to how many cells were counted in the larger wells used in manual counting, it was likely not a question of space but rather of access to nutrients from the medium that limited the growth in the 96-well plates.

The Western blot analyses showed a few different things. As stated in the Results, the first blot showed that the amount of p-ERK was not dependent on the trametinib concentration, in either cell line, when the cells were treated for 72 hours.

The second blot (figure 1) showed similar results as the study on which the treatment regimen was based (36). This blot only included A549 cells. First, when treating with increasing trametinib concentrations for a fixed time of 24 hours, there was a slight decrease in p-ERK. However, this effect was not very distinct. More clear was that when treating the cells with the same trametinib concentration for different timepoints, the amount of p-ERK was lower for shorter durations and increased after 8 hours. This kind of p-ERK rebound after treatment with MEK inhibitors has been shown previously (36, 37), and has been explained by the interruption of negative feedback loops in which p-ERK is involved (37, 38). When, at first, the amount of p-ERK decreases, the inhibiting effect it has exerted upstream in the MAPK pathway is lifted, thereby further activating this

pathway from high up in the chain. This leads to more activated MEK, and thus the rebound in p-ERK. In our study, this rebound effect helps explain why there was no dose-dependency shown in the first blot, where the cells were treated for 72 hours. It can also contribute to the weak p-ERK decrease and dose-dependency shown in the 24 hour treatment (A549 cells). While (36) had a very distinct decrease in p-ERK when treating A549 with increasing trametinib concentrations, this study also showed a later onset of the rebound – the amount of p-ERK had not started to increase after 12 hours, and rebound was first shown after 24 hours. In our case, there was a rebound in p-ERK already after 8 hours, which would indicate that after 24 hours of treatment there has also been several hours of rebound.

While the results discussed above have been shown before, it was unexpected that the controls in the blot (0 nM and 0 hours of treatment, respectively) showed so little p-ERK. This is especially noticeable for the 0 nM control; here, close to no p-ERK is found. This can not be explained by issues with loading, as shown by the blotting for actin. In light of this, it seems that trametinib induces phosphorylation of ERK, as each treated sample has a higher level of p-ERK than the corresponding control. However, this is not consistent with the action of trametinib as a MEK inhibitor, preventing ERK phosphorylation, nor can it be explained via the p-ERK rebound that has been shown. While trametinib treatment can result in p-ERK *rebound*, this relies on feedback loops in which p-ERK exerts an inhibiting role on the MAPK pathway. This means that the control cells should never have low amounts of p-ERK; if they indeed did, the feedback loops would kick in and activate the pathway upstream of ERK, resulting in more p-ERK. Other studies have also shown high amounts of p-ERK in non-treated A549 cells (36, 37). Thus, it is likely that these unexpected results were due to handling errors. In the discussion above it has been assumed that non-treated A549 cells contain distinct levels of p-ERK, but the experiment should be repeated to confirm this assumption.

The focus of the study was that of the potency of trametinib in 2D and 3D. As stated in the Results above, no difference between the environments nor between the cell lines was shown (see also table 2). As the cancerous A549 cells carry a KRAS mutation that leaves their MAPK pathway constitutively active and contributing to their proliferation, we expected to see a larger effect of the treatment in these cells compared to the non-cancerous LL47. This kind of specific targeting was not shown in the potency. However, it would be of interest to investigate the IC_{50} values of trametinib in the cell lines, both to see if this differs but also to see the maximum absolute inhibitory effect trametinib can elicit. It is of course possible that even though trametinib is equally potent in both cell lines, it is more efficacious in the A549 cells.

This kind of investigation would also be interesting for comparing the 2D vs 3D, as previous studies have shown differences in the IC_{50} values when testing compounds in different environments. While the potency of trametinib remained the same in both models, there were some other interesting differences. For the LL47 cells, the dose-dependency data points in 3D adhered more closely to the theoretical model, when comparing to the 2D values (see figures 3 and 5). This suggests that this cell line relies more on its MAPK pathway in a 3D environment: in 2D, the response was less predictable and could be due to some cells responding and some not, i.e. not all

cells relying on this pathway, while in 3D it seemed there was a more uniform response. The results in 3D were also more reproducible. It should also be taken into account that more cells were seeded in 3D. While the area is much larger due to the membrane, this could still give more inter-cell signalling if the cells aggregate, and result in more proliferation as compared to 2D. In other words, it could be the case that the LL47 cells grew slower in the 2D environment, with a generally less activated MAPK pathway, compared to the 3D environment. This shift to a more active MAPK pathway when cells are cultured in 3D has been shown for other cell lines (39). However, those cell lines in question were cancerous, and the 3D environment was more complex than in this study. Thus, the results cannot be directly applied to our case.

For the A549 cells, there was another difference to note between the 2D and 3D experiments: with the exception of the highest trametinib concentration, which in any case was disregarded as an outlier, the dose-dependency curves plateaued in a more distinct way from around 1-3 µM in 3D, while in 2D such a plateau was not seen (see figures 2 and 4). One advantage of a 3D environment is that it allows the cells to form a tumour-like aggregate, which would not be supported in 2D (40). Such an aggregate could explain the observed plateau, since, much like in *in vivo* tumours, diffusion into the aggregate would be limited (41, 42). This could mean that the inner cell layers would not get the same dose trametinib, but instead receive much lower levels compared to the treatment any outer cell layer would get. This in turn could mean that while an increasing trametinib concentration exerts more and more of an inhibitory effect on the outer cell layers, the inner cells remain unaffected by the increasing dose. Thus, only some cell layers are inhibited, giving the decreased signal in the assay, but at some point, when these have been virtually completely inhibited, we continue to receive the same signal from the inner cells, regardless of the trametinib concentration. It has also been shown that due to this general limited transport, this kind of tumour-like cell aggregates display distinct zones, where the outer layer is the only one proliferating and with an inner layer that is quiescent (43, 44). This would explain the results in a slightly different way: if only the outer layer is proliferating, these are the only cells that would be affected by the trametinib. Even if the compound would be able to penetrate the aggregate and reach the inner cells, they would be in a viable but quiescent state, meaning that they would not proliferate regardless of the trametinib treatment. Thus, like explained above, once the outer cell layer was fully inhibited, the signal would plateau on the level provided by the inner cells. It would be of interest to investigate whether we indeed have this kind of tumour-formation in the 3D model, to confirm or deny this suggested explanation for the plateau. Another important aspect to consider in this case is the use of the WST-1 assay, which relies on reagents entering the cells. While this assay is very quick and easy to perform, if diffusion to the cells is limited, another viability assay could be more accurate.

As has been mentioned both in the results and earlier in the discussion, in 2D the highest trametinib concentration (100 µM) often gave a higher signal (that is, lower inhibition) than the second highest concentration (30 µM) and was not taken into account when the data points were used to construct the dose-dependency curves. A very likely explanation for this is the low water-solubility of trametinib. The trametinib might have precipitated in the medium when it was added

to the cells. In fact, in 2D, something that very much resembled precipitation was indeed observed in the wells treated with this concentration. This affects the generated signal in two ways. Firstly, if the trametinib precipitates it does not enter the cells and thus cannot exert any inhibitory effect. Secondly, the precipitation itself may directly interfere with the absorbance readings, as it forms opaque particles. What is interesting to note is that this effect is not shown in 3D. However, in 3D the signals from these wells were still removed when constructing the dose-dependency curves, as the signal in general had plateaued much earlier, as previously discussed. As the medium was transferred from the 3D plate before the absorbance was read, it is possible that any precipitates were left behind and thus they could not interfere directly with the absorbance as described above.

Leaving behind the comparisons to the 2D model, the 3D model in itself proved to be a working one. While there were a few added steps before the cells could be seeded, and an extra step of transferring the medium for WST-1 analysis, this was not a major inconvenience, and the model gave reproducible results. Given the advantages of a 3D model highlighted in the Introduction, the use of this model should be incorporated into more *in vitro* work.

Acknowledgements

This study was performed as a degree project at Red Glead Discovery. I would like to thank Red Glead for this opportunity, with special thanks to Martina Kvist Reimer, Reihaneh Zarrizi and Mahtab Azimi for all their input, advice, and encouragement along the way. I would also like to thank all my colleagues at Red Glead for providing a pleasant and supportive work environment.

Furthermore, I would like to thank my supervisor at LTH, Malin Lindstedt, for her help and quick answers throughout the project.

Lastly, a special thank you to my mum, for her unwavering, ubiquitous support. This report would not have existed without her.

References

1. Ferlay, J., M. Colombet, I. Soerjomataram, C. Mathers, D. M. Parkin, M. Piñeros, A. Znaor, and F. Bray. 2019. Estimating the global cancer incidence and mortality in 2018: GLOBOCAN sources and methods. *Int J Cancer* 144: 1941-1953.
2. Hanahan, D., and R. A. Weinberg. 2011. Hallmarks of cancer: the next generation. *Cell* 144: 646-674.
3. Alberts, B., D. Bray, K. Hopkin, A. Johnson, J. Lewis, M. Raff, K. Roberts, and P. Walter. 2014. *Essential Cell Biology*. Garland Science, New York, NY.
4. Weinstein, I. B. 2002. Cancer. Addiction to oncogenes--the Achilles heal of cancer. *Science* 297: 63-64.
5. Weinstein, I. B., and A. Joe. 2008. Oncogene addiction. *Cancer Res* 68: 3077-3080; discussion 3080.
6. A Boelsterli, U. 2003. *Mechanistic Toxicology*. Taylor & Francis, Abingdon, England.
7. Brancato, V., J. M. Oliveira, V. M. Correlo, R. L. Reis, and S. C. Kundu. 2020. Could 3D models of cancer enhance drug screening? *Biomaterials* 232: 119744.
8. Hutchinson, L., and R. Kirk. 2011. High drug attrition rates--where are we going wrong? *Nat Rev Clin Oncol* 8: 189-190.
9. Unger, C., N. Kramer, A. Walzl, M. Scherzer, M. Hengstschläger, and H. Dolznig. 2014. Modeling human carcinomas: physiologically relevant 3D models to improve anti-cancer drug development. *Adv Drug Deliv Rev* 79-80: 50-67.
10. Shuford, S., C. Wilhelm, M. Rayner, A. Elrod, M. Millard, C. Mattingly, A. Lotstein, A. M. Smith, Q. J. Guo, L. O'Donnell, J. Elder, L. Puls, S. J. Weroha, X. Hou, V. Zanfagnin, A. Nick, M. P. Stany, G. L. Maxwell, T. Conrads, A. K. Sood, D. Orr, L. M. Holmes, M. Gevaert, H. E. Crosswell, and T. M. DesRochers. 2019. Prospective Validation of an Ex Vivo, Patient-Derived 3D Spheroid Model for Response Predictions in Newly Diagnosed Ovarian Cancer. *Sci Rep* 9: 11153.
11. Aoudjit, F., and K. Vuori. 2001. Integrin signaling inhibits paclitaxel-induced apoptosis in breast cancer cells. *Oncogene* 20: 4995-5004.
12. Kim, Y.-J., H.-I. Bae, O. K. Kwon, and M.-S. Choi. 2009. Three-dimensional gastric cancer cell culture using nanofiber scaffold for chemosensitivity test. *International Journal of Biological Macromolecules* 45: 65-71.
13. Abe-Fukasawa, N., K. Otsuka, A. Aihara, N. Itasaki, and T. Nishino. 2018. Novel 3D Liquid Cell Culture Method for Anchorage-independent Cell Growth, Cell Imaging and Automated Drug Screening. *Sci Rep* 8: 3627.
14. Patra, B., M. A. Lateef, M. N. Brodeur, H. Fleury, E. Carmona, B. Péant, D. Provencher, A. M. Mes-Masson, and T. Gervais. 2020. Carboplatin sensitivity in epithelial ovarian cancer cell lines: The impact of model systems. *PLoS One* 15: e0244549.
15. Mas, C., B. Boda, M. CaulFuty, S. Huang, L. Wiszniewski, and S. Constant. 2015. Antitumour efficacy of the selumetinib and trametinib MEK inhibitors in a combined human airway-tumour-stroma lung cancer model. *J Biotechnol* 205: 111-119.
16. Muguruma, M., S. Teraoka, K. Miyahara, A. Ueda, M. Asaoka, M. Okazaki, T. Kawate, M. Kuroda, Y. Miyagi, and T. Ishikawa. 2020. Differences in drug sensitivity between two-dimensional and three-dimensional culture systems in triple-negative breast cancer cell lines. *Biochem Biophys Res Commun* 533: 268-274.
17. Raghavan, S., M. R. Ward, K. R. Rowley, R. M. Wold, S. Takayama, R. J. Buckanovich, and G. Mehta. 2015. Formation of stable small cell number three-dimensional ovarian cancer spheroids using hanging drop arrays for preclinical drug sensitivity assays. *Gynecol Oncol* 138: 181-189.
18. Sun, T., S. Jackson, J. W. Haycock, and S. MacNeil. 2006. Culture of skin cells in 3D rather than 2D improves their ability to survive exposure to cytotoxic agents. *J Biotechnol* 122: 372-381.

19. Dhiman, H. K., A. R. Ray, and A. K. Panda. 2005. Three-dimensional chitosan scaffold-based MCF-7 cell culture for the determination of the cytotoxicity of tamoxifen. *Biomaterials* 26: 979-986.
20. Sowa, M. B., W. B. Chrisler, K. D. Zens, E. J. Ashjian, and L. K. Opresko. 2010. Three-dimensional culture conditions lead to decreased radiation induced cytotoxicity in human mammary epithelial cells. *Mutat Res* 687: 78-83.
21. Doillon, C. J., E. Gagnon, R. Paradis, and M. Koutsilieris. 2004. Three-dimensional culture system as a model for studying cancer cell invasion capacity and anticancer drug sensitivity. *Anticancer Res* 24: 2169-2177.
22. Pampaloni, F., E. G. Reynaud, and E. H. Stelzer. 2007. The third dimension bridges the gap between cell culture and live tissue. *Nat Rev Mol Cell Biol* 8: 839-845.
23. Lim, S. H., and H. Q. Mao. 2009. Electrospun scaffolds for stem cell engineering. *Adv Drug Deliv Rev* 61: 1084-1096.
24. Ma, Z., M. Kotaki, R. Inai, and S. Ramakrishna. 2005. Potential of nanofiber matrix as tissue-engineering scaffolds. *Tissue Eng* 11: 101-109.
25. Antoni, D., H. Burckel, E. Josset, and G. Noel. 2015. Three-dimensional cell culture: a breakthrough in vivo. *Int J Mol Sci* 16: 5517-5527.
26. Malakpour Permlid, A., P. Roci, E. Fredlund, F. Falt, E. Onell, F. Johansson, and S. Oredsson. 2019. Unique animal friendly 3D culturing of human cancer and normal cells. *Toxicol In Vitro* 60: 51-60.
27. Bazzolo, B., E. Sieni, A. Zamuner, M. Roso, T. Russo, A. Gloria, M. Dettin, and M. T. Conconi. 2020. Breast Cancer Cell Cultures on Electrospun Poly(ε-Caprolactone) as a Potential Tool for Preclinical Studies on Anticancer Treatments. *Bioengineering (Basel)* 8.
28. Malakpour-Permlid, A., I. Buzzi, C. Hegardt, F. Johansson, and S. Oredsson. 2021. Identification of extracellular matrix proteins secreted by human dermal fibroblasts cultured in 3D electrospun scaffolds. *Sci Rep* 11: 6655.
29. Tridente, G. 2017. Trametinib. In *Adverse events and oncotargeted kinase inhibitors*. Elsevier Inc. 531-559.
30. L Patrick, G. 2017. *An Introduction to Medicinal Chemistry*. Oxford University Press, Oxford, United Kingdom.
31. Sato, H., H. Yamamoto, M. Sakaguchi, K. Shien, S. Tomida, T. Shien, H. Ikeda, M. Hatono, H. Torigoe, K. Namba, T. Yoshioka, E. Kurihara, Y. Ogoshi, Y. Takahashi, J. Soh, and S. Toyooka. 2018. Combined inhibition of MEK and PI3K pathways overcomes acquired resistance to EGFR-TKIs in non-small cell lung cancer. *Cancer Sci* 109: 3183-3196.
32. Klymkowsky, M. W., and P. Savagner. 2009. Epithelial-mesenchymal transition: a cancer researcher's conceptual friend and foe. *Am J Pathol* 174: 1588-1593.
33. Holder, A. M., A. Akcakanat, F. Adkins, K. Evans, H. Chen, C. Wei, D. R. Milton, Y. Li, K. A. Do, F. Janku, and F. Meric-Bernstam. 2015. Epithelial to mesenchymal transition is associated with rapamycin resistance. *Oncotarget* 6: 19500-19513.
34. Wang, B., N. Ma, X. Zheng, X. Li, X. Ma, J. Hu, and B. Cao. 2020. GDF15 Repression Contributes to 5-Fluorouracil Resistance in Human Colon Cancer by Regulating Epithelial-Mesenchymal Transition and Apoptosis. *Biomed Res Int* 2020: 2826010.
35. Li, M., H. Chen, T. Sun, Z. Ma, X. Chen, D. Wu, W. Huang, and X. Wang. 2020. p70S6K Promotes Acquired Resistance of Erlotinib Through Induction of Epithelial-Mesenchymal Transition in Non-Small Cell Lung Carcinoma. *Onco Targets Ther* 13: 5257-5270.
36. Dai, X., H. Xia, S. Zhou, Q. Tang, and F. Bi. 2019. Zoledronic acid enhances the efficacy of the MEK inhibitor trametinib in KRAS mutant cancers. *Cancer Lett* 442: 202-212.
37. Lito, P., A. Saborowski, J. Yue, M. Solomon, E. Joseph, S. Gadal, M. Saborowski, E. Kastenhuber, C. Fellmann, K. Ohara, K. Morikami, T. Miura, C. Lukacs, N. Ishii, S. Lowe, and N. Rosen. 2014. Disruption of CRAF-mediated MEK activation is required for effective MEK inhibition in KRAS mutant tumors. *Cancer Cell* 25: 697-710.

38. Dougherty, M. K., J. Müller, D. A. Ritt, M. Zhou, X. Z. Zhou, T. D. Copeland, T. P. Conrads, T. D. Veenstra, K. P. Lu, and D. K. Morrison. 2005. Regulation of Raf-1 by direct feedback phosphorylation. *Mol Cell* 17: 215-224.
39. Gangadhara, S., C. Smith, P. Barrett-Lee, and S. Hiscox. 2016. 3D culture of Her2+ breast cancer cells promotes AKT to MAPK switching and a loss of therapeutic response. *BMC Cancer* 16: 345.
40. Edmondson, R., J. J. Broglie, A. F. Adcock, and L. Yang. 2014. Three-dimensional cell culture systems and their applications in drug discovery and cell-based biosensors. *Assay Drug Dev Technol* 12: 207-218.
41. Ward, J. P., and J. R. King. 2003. Mathematical modelling of drug transport in tumour multicell spheroids and monolayer cultures. *Math Biosci* 181: 177-207.
42. Curcio, E., S. Salerno, G. Barbieri, L. De Bartolo, E. Drioli, and A. Bader. 2007. Mass transfer and metabolic reactions in hepatocyte spheroids cultured in rotating wall gas-permeable membrane system. *Biomaterials* 28: 5487-5497.
43. Mehta, G., A. Y. Hsiao, M. Ingram, G. D. Luker, and S. Takayama. 2012. Opportunities and challenges for use of tumor spheroids as models to test drug delivery and efficacy. *J Control Release* 164: 192-204.
44. Khaitan, D., S. Chandna, M. B. Arya, and B. S. Dwarakanath. 2006. Establishment and characterization of multicellular spheroids from a human glioma cell line; Implications for tumor therapy. *J Transl Med* 4: 12.

All degree project courses at LTH currently include writing a popular science summary of the longer project report. The summary of this report can be found on the following page.

2D vs 3D models – the point and effects of adding a third dimension in cancer research

The battle against cancer is an ongoing one, not just for individual patients, but for the pharmaceutical industry at large. To efficiently test new drug candidates, it is important to use accurate models. In this study, one model that is thought to provide some of this accuracy – a three-dimensional electrospun membrane – was investigated. While drug potency remained the same as in a more traditional model, some other interesting differences were revealed. All-in-all, the notion that this model has the potential to be used in drug development was supported.

Long before reaching any human trials, new potential drugs are tested in so called *in vitro* models. This typically involves testing the drug candidates on cells grown on flat, two-dimensional (2D) surfaces. While this method has been – and continues to be – very useful, it also has several flaws. A big concern is that the 2D environment this method provides is nothing like the three-dimensional (3D) environment of the human body. This may result in the cells behaving differently, and a drug candidate that seem promising in 2D tests may be useless for actually treating the disease in a patient. To combat this issue, more and more attention has been put on newer 3D models. In such models, the cells can grow in three dimensions, more like they would do naturally. Many studies have shown that cells are less sensitive to drugs in this kind of model, when comparing to a traditional 2D one. One example of a 3D model is electrospun membranes, which consist of very thin fibres that can be oriented in different ways. These membranes aim to mimic the extracellular matrix (ECM), which can be thought of as a scaffold to which the cells are attached in the body. In our study, this was the 3D model used for comparing 2D and 3D environments.

Of course, while there is a need for new cancer drugs, there are already working ones on the market. One drug that is used against certain cancers is trametinib. Trametinib inhibits MEK, an enzyme which is a part of the so called MAPK pathway, which is involved in cell growth and proliferation. Here, trametinib was used to treat the cells to see if the potency changed when going from a 2D to a 3D model. The cells used were human cancerous A549 cells, and human non-cancerous LL47 cells. The A549 cells have a mutation that results in their MAPK pathway always being active.

No potency change could be seen, neither between the different cells, nor when going from the 2D to the 3D model. However, there were some other changes of interest. Firstly, the non-cancerous LL47 cells seemed more reliant on their MAPK pathway in 3D. This is a hint that they do indeed behave differently in the different models. Secondly, the cancerous A549 cells showed a result in 3D that might indicate that they formed a tumour-like aggregate in this model. This is an advantage of a 3D model, as it mimics the tumours found in the body. Of course, further studies investigating this possible tumour-formation would be useful to confirm or deny this theory.

Leaving the 2D vs 3D comparison behind, the 3D model itself proved to be easy to work with and give reproducible results. Given the known advantages of 3D models in general, and in line with studies done by others, this highly suggests that this model should be included in more studies of new anti-cancer drugs.